Pulse Propagation Characteristics at 2.4 GHz Inside Buildings

Seong-Cheol Kim, Henry L. Bertoni, *Fellow, IEEE*, and Miklos Stern, *Member, IEEE*

Abstract—**The growing use of unlicensed wireless systems has spurred interest in the 2.4-GHz ISM band. In order to facilitate the design of such systems, measurements of the pulse response characteristics have been made inside commercial buildings. From the measured pulse response, the statistical properties of the amplitude variation for individual pulses was determined, in addition to path loss, mean excess delay, root mean square (rms) delay spread, and the coherence bandwidth of the indoor channel.**

I. Introduction

ANALYSIS of the radio communication channel characteristics is important for the development of wireless systems such as personal communication systems (PCS), wireless private branch exchanges (PBX), and wireless local area networks (LAN). Narrow band or continuous wave (CW) path loss is a parameter that can predict the power level of the system and the space coverage of the base station, while impulse response parameters such as mean excess delay and root mean square (rms) delay spread are useful to obtain the bit error rate (BER) and the data rate. The technical literature has many reports on CW propagation loss and impulse response measurements in the 800-, 850-, and 900-MHz bands and 1.3-, 1.5-, and 1.8-GHz bands [1]–[13], [16].

The increasing demand for wireless systems that do not require licensing has motivated us to investigate indoor impulse channel characteristics in the 2.4-GHz ISM band. The measurements employed a 2.4-GHz carrier that was modulated by repetitive 5-ns pulses and transmitted through an wideband biconical antenna. The received signal is demodulated by an envelop detector, which has a 22-dB dynamic range. Impulse response measurements were made in two buildings: an engineering building with typical office and laboratory areas and a large retail store building having a storage area and a sales floor.

From the measured data, the impulse response parameters and their statistics were obtained and the coherence bandwidth was calculated from the average power delay profile. Individual peak amplitude statistics are also presented to help understand the multipath interference and its variations with small changes in the receiver position.

Manuscript received June 12, 1995; revised September 22, 1995. This work was supported in part by a grant from Symbol Technologies, Inc. and in part by the New York State Science and Technology Foundation.

S.-C. Kim and H. L. Bertoni are with the Center for Advanced Technology in Telecommunications, Polytechnic University, Brooklyn, NY 11201 USA.

M. Stern is with the R&D Department, Symbol Technologies, Inc., Bohemia, NY 11716 USA.

Publisher Item Identifier S 0018-9545(96)05468-0.

II. Description of the Measurements

A. Measurement System

The measurement system for obtaining the impulse response is shown in Fig. 1. The transmitter consists of an oscillator, a mixer, a pulse-generator, and a power-amplifier. The 2.4-GHz carrier generated by the oscillator is modulated in the mixer by the 5-ns square pulse whose repetition period is 500 ns. The modulated signal has a bandwidth of about 200 MHz and an on/off ratio of 26 dB. It is amplified to 28 dBm by the power amplifier and radiated between a pair of biconical antennas that have very wide bandwidth (>200 MHz) and an omnidirectional radiation pattern in the horizontal plane. The height of the transmitting antenna is usually fixed to be above furniture, merchandise shelves, and other scatterers, and is located near the center of the building being surveyed.

The received signal is first fed through a precision variable attenuator that is adjusted so that the sum of the propagation loss and attenuator loss is about 98 dB. This implies that the transmitter and the receiver pair can provide the reliable response with up to 98-dB propagation loss between them. The receiver consists of two low noise amplifiers followed by a bandpass filter (BW = 200 MHz) and an envelope detector, which is connected to the digital sampling scope (Tektronix TDS540) through a video amplifier stage. In order to synchronize the receiver to the transmitter, the oscilloscope is triggered through a cable connection by the sync output channel of the pulse generator, which has a delay adjustment relative to the time of the output pulse. Note that the synchronization procedure used precludes the measurement of absolute propagation delay. The vertical and horizontal settings of the scope were kept constant during the entire measurement sequence, and the scope was run in the 100× average mode to improve the signal to noise ratio. Amplifier nonlinearity and thermal noise limit the dynamic range of the impulse response to 22 dB. A portable computer with an IEEE-488 interface card controls the digital sampling scope and collects the data in the form of voltage as a function of time at 0.1-ns intervals over 500 ns. While the effect of the operator's body on the received signal level will be significant for handheld units, we have chosen to mount the receiving antenna on an industrial cart in order to standardize the measurements and to permit comparison between different receiver positions. The

0018–9545/96$05.00 © 1996 IEEE

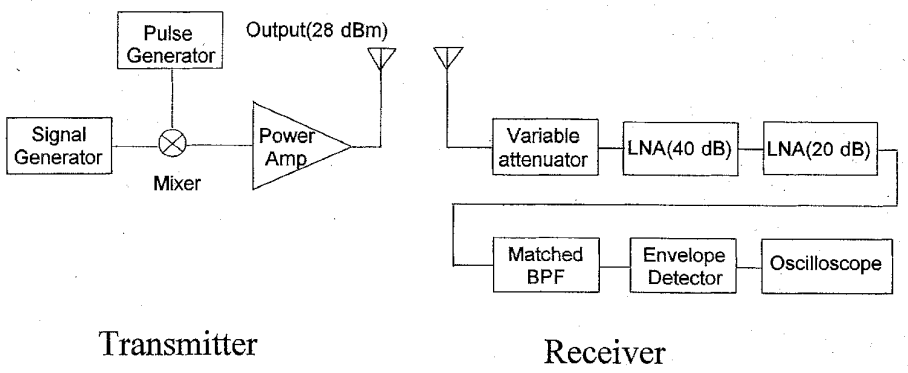

Fig. 1. Block diagram of impulse response measurement system.

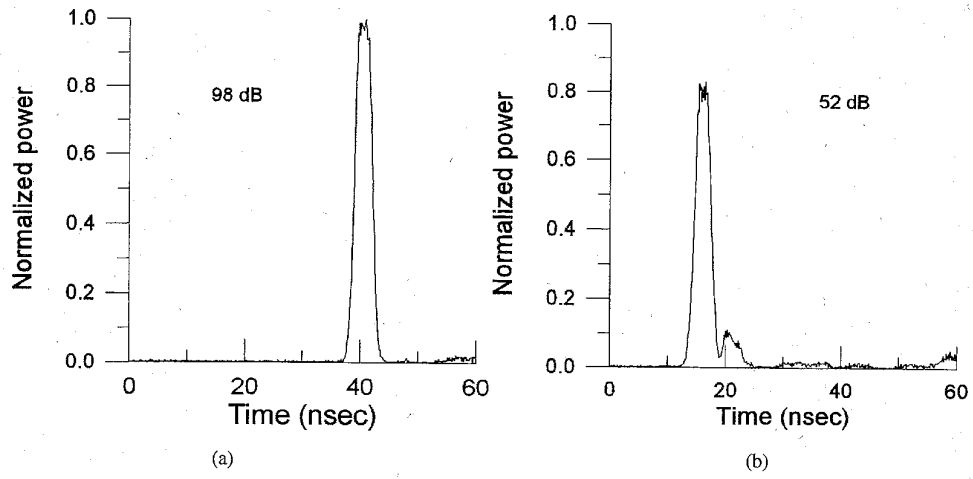

Fig. 2. Reference impulse response measurement. (a) Direct connection. (b) 10 λ separation.

receiving antenna is secured to a wooden base that is affixed to a fiberglass pole tied to the cart. The antenna height of 1.42 m above the floor is typical of handheld mobile radio units in a wireless LAN environment and is high enough to avoid blockage of the signal path by the industrial cart and the receiver equipment on it.

Calibration measurements were made using direct cable connection of the transmitter and the receiver through the calibrated attenuator in order to allow the feed-through and the nonlinearities to be removed by processing the raw data obtained from the measurements. Antenna gain was also removed using a calibration measurement with the antennas separated by 10λ in a large open area. The shape of the received signal for a direct cable connection between the transmitter and the receiver is rounded off due to the limited bandwidth (200 MHz) of the measurement system as shown in Fig. 2(a), where the time origin is a function of delay settings and does not represent the starting time of the transmitted pulse. The rms pulse duration of the measured probing pulse is 1.52 ns while the 3-dB pulse duration is 3.2 ns. Since the bandwidth of the biconical antennas is significantly wider than 200 MHz, the shape of the primary received pulse is not changed when the signal is propagated between the antennas in free space, as is seen by comparing the main pulse in Fig. 2(b) to that in Fig. 2(a).

B. Building Environments

Experiments were carried out in two different types of building. The first was a typical engineering building consisting of a large open area divided into cubicles by head high movable partitions. This area is surrounded by rooms of different sizes, some of which are engineering laboratories. Fig. 3 shows the layout of the building whose size is 60.5 by 44 m. The external walls of this building are made of concrete-blocks and the internal walls of gypsum board on metal studs. The partitions in the cubicle section are 1.57 m high and made of wood and fabric with metal frame. The laboratories contain wooden benches with metal shelves holding lab-equipment and metal cabinets. The other rooms contain standard office furniture. The nonmetallic acoustic ceiling tiles are supported by a $4'$ by $2'$ metal grid 2.9 m above the floor, which is made of concrete and covered with carpets. The transmitter was located at a cross isle between the cubicles near the center of the main cubicle area at a height of 2.5 m.

The second building was a large retail store having an open sales floor with storage and facilities rooms at the

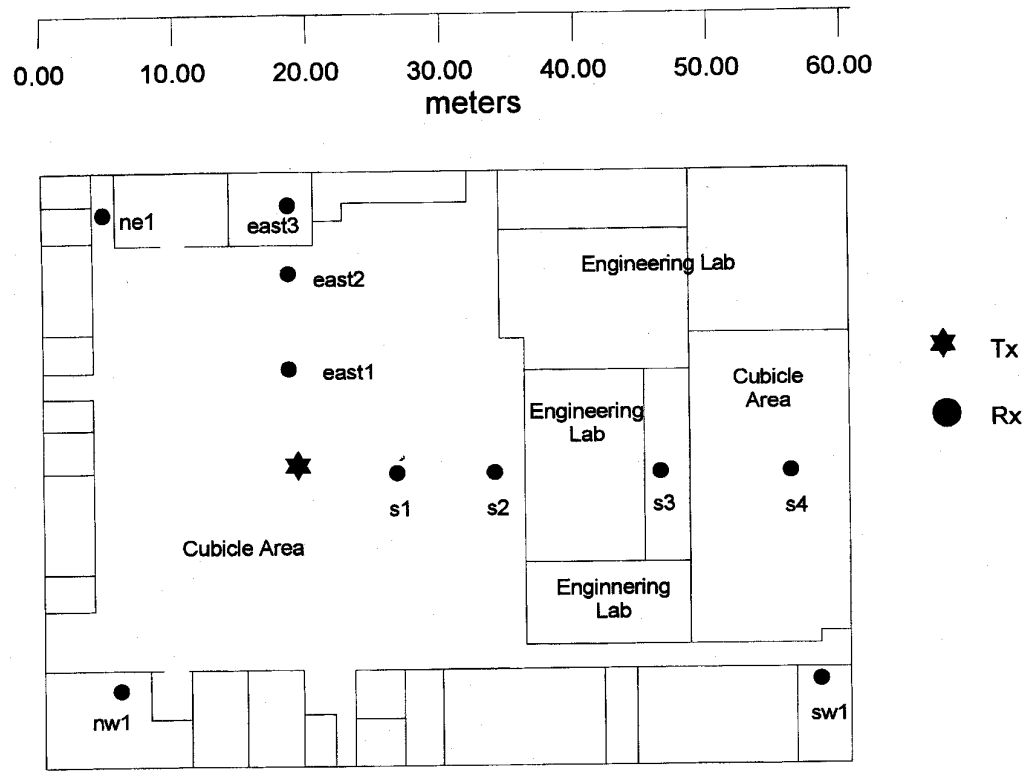

Fig. 3. Floor plan of Engineering building.

back of the building. Fig. 4 shows the layout of the store and the transmitter and the receiver locations used for the measurements. The building is almost square with dimensions 100.5 m (330 ft) by 108.5 m (356 ft). Both interior and exterior walls are made of concrete blocks except for the 64-m-long (210 ft) glass wall at the entrance to the building. The building has a 5.28-m-high metal roof, supported by the metal columns shown in Fig. 4. A metal structure supporting the roof and utility pipes extends below the roof to a height of 4.72 m above the floor over the entire building. The dropped ceiling in the sales floor area is made of nonmetallic acoustic tiles supported by a $4' \times 2'$ metal grid and is about 4.27 m above the floor. There is no drop ceiling in the storage room. Two thirds of the sales floor has nonmetallic shelves supported by metal frames of various heights ranging from 1.82 to 2.3 m and filled with a variety of metallic and nonmetallic sales items. The other parts of the sales floor have various kinds of metal racks and glass display cases whose heights are from 1 to 1.5 m. Metal frame shelves between 1.82 and 2.44 m high are located in the storage room and are filled with merchandise up to 3.35 m. The transmitter was placed near the center of the building on the top of a merchandise shelf at a height of 2.95 m.

C. Experimental Procedure

A total of ten receiver sites in the engineering building and seven sites in the retail store were chosen for measurements. In the engineering building shown in Fig. 3, four sites in the main cubicle area have a line-of-sight (LOS) path to the transmitter. For three sites located in the room or the corridor surrounding the main cubicle area, a single wall separates the receiver and transmitter, while the remaining three sites are separated by two or more walls. The receiver site located in the engineering laboratory is heavily cluttered by scatterers.

In the retail store of Fig. 4, four out of five sites on the sales floor have the path to the transmitter obstructed by the merchandise shelves. Two of these sites have light surrounding clutter whose height is comparable to that of the receiving antenna, and another two are heavily cluttered by the merchandise shelves. The remaining site in the sales floor has a LOS path to the transmitter, although there is a metal pole that is slightly off center from the direct line between the transmitter and the receiver. For one receiver site located in the storage room, the direct path is blocked by a wooden door with spring loaded hinges. The other site in the storage room has a heavily cluttered environment of densely loaded merchandise shelves. At this site there is a concrete block wall blocking the LOS path between the transmitter and the receiver.

At each measurement site, the receiver was located at 16 different positions separated by one quarter wavelength in order to examine the fast-fading variations of the received signal resulting from multipath interference. At each position the impulse response was recorded with the help of a portable computer for subsequent processing, as previously described. Because the measurements were made in isles between partitions or merchandise shelves, the 16 points were for convenience located along a straight line in center of the isle. Since the Turin multipath model [13] suggests that the fast fading pattern has the same statistical properties for all choice

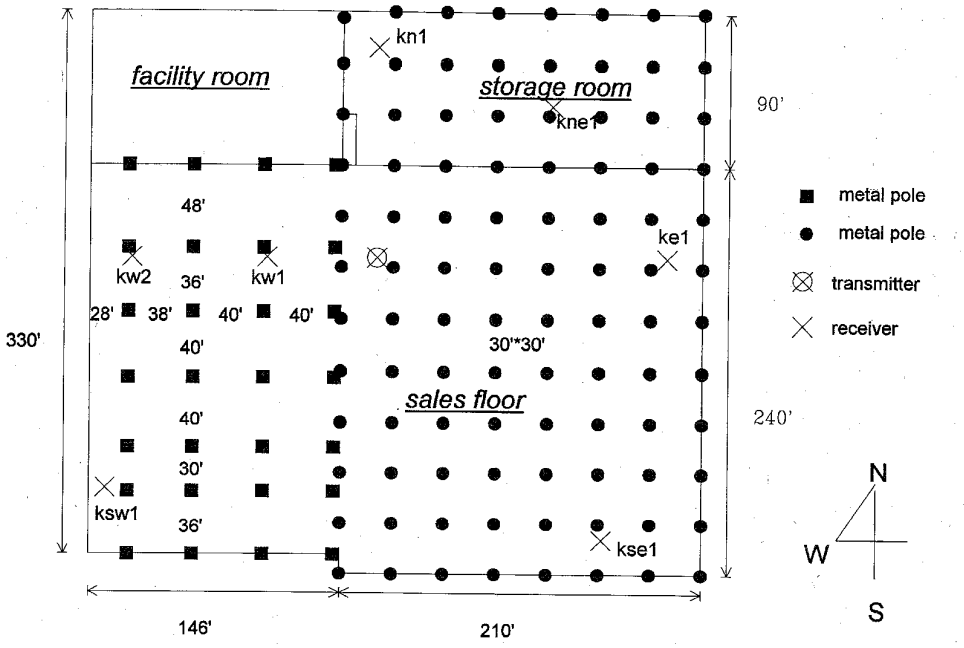

Fig. 4. Floor plan of retail store building.

of receiver displacement, no information is lost by locating the receiver points along a straight line. For measurement sites with an LOS path in the engineering building, the straight line of the receiver location was parallel to the direct path to the transmitter, while for all the remaining sites it was perpendicular or at an angle to the direct path. For all 16 measurements at the site, the attenuator was set at the same value.

III. Overview of Measured Pulse Response

A. Power Delay Profile

Power delay profiles obtained from measured pulse responses can be separated into three different categories. The first category applies when a LOS path exists between the transmitter and the receiver, the second category consists of lightly obstructed paths, and the third category is for heavily obstructed paths. A series of typical power delay profile $s(t)$ for those three groups are shown in Figs. 5–8.

Fig. 5(a) and (b) shows power delay profiles for the site "east1" in the engineering building, where the receiver has a LOS path to the transmitter. The receiving antenna was located in the center of the passage way between cubicles and was at a distance of 7.32 m (24 ft) from the transmitter. The first dominant pulse in Fig. 5(a) appears to arise from the signal traveling over a single path, but it is actually composed of two subpaths as seen in Fig. 5(b), when the receiver is moved two wavelengths along the straight line parallel to the direct line between the transmitter and the receiver. The signal strengths of the split pulses in Fig. 5(b) are weaker than that of the merged pulse in Fig. 5(a), implying that pulses from two subpaths interfere constructively. Based on the heights of two antennas and their separation, it appears that the first and the second subpaths correspond to the direct and the floor reflected paths, respectively.

A third pulse, evident in Fig. 5(b) near 10 ns, is negligible in Fig. 5(a). The signal strength of this pulse is even stronger than that of the first perceptible path of Fig. 5(b). Conversely, the strong echo at 20 ns in Fig. 5(a) is weaker than other scattered pulses in Fig. 5(b). These results imply that even for a LOS path to the transmitter, what appear to be individual pulses are actually composed of multipath signals so that the pulse amplitude strongly depends on the phase differences between subpaths, which change as a result of moving the receiver. This observation is contrary to the claim of reference [10] that "multipath components fade very slightly with small movement of the receiver, granting that the first perceptible pulse seldom varies in regard to this small movement."

Two representative pulse responses in the retail store are shown in Figs. 5(c) and (d) for the site "ke1," which has a LOS path to the transmitter. The environment contains vertical support columns that are slightly off centered from the direct line between the transmitter and the receiver, which are separated by 47.85 m (157 ft). In addition, low-height metal shelves partially block the LOS path for a few of 16 different measurement points at this particular site. Fig. 5(c) shows the pulse response for a partially blocked LOS path, while 5(d) is the pulse response at a distance 21.5 cm away along the straight line perpendicular to the direct line between the transmitter and the receiver, where there is a clear LOS path. The strength of the first pulse in Fig. 5(c) differs from that in 5(d) by about 7.3 dB, which is a result of partial obstruction of the direct path. The first pulse in Fig. 5(c) and (d) is a superposition of the direct path and the floor reflected path, whose differential delay is small for this large antenna separation. The nearest wall is 14.63 m (48 ft) away from

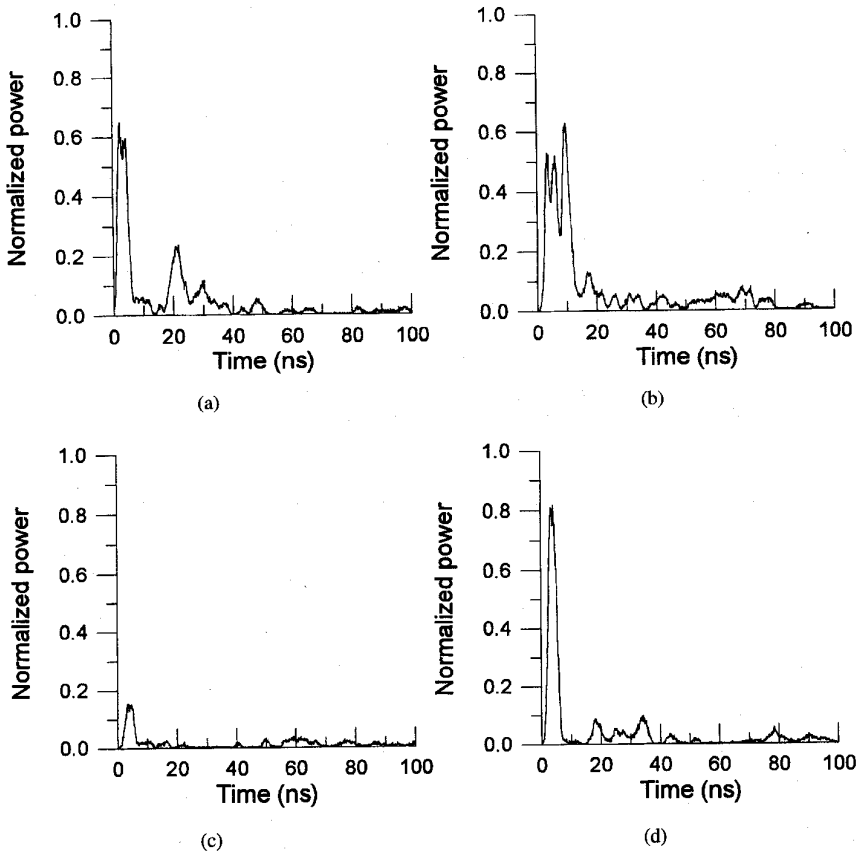

Fig. 5. Power delay profiles for sites with LOS paths to the transmitter (a) and (b) in the engineering building and (c) and (d) in the retail store.

the receiver. Reflection from the wall gives rise to the pulse seen near 50 ns in Fig. 5(c) and (d), and its strength is seen to be relatively weak compared with other scattered pulses. For the LOS paths both in the engineering building and in the retail store, pulses arriving with substantial amplitudes are concentrated in the early time of the response, which results in small mean excess delay.

Power delay profiles corresponding to the lightly obstructed category are shown in Fig. 6(a)–(c) for the site "ne1" in the engineering building (see Fig. 3). At this site the direct path to the transmitter is blocked by the gypsum board wall of the room adjacent to the measurement site, although reflected rays reach the receiver without going through walls. The receiver position of Fig. 6(b) is one wavelength (12.3 cm) away from the position of 6(a), and that of 6(c) another one and a quarter wavelength (15.4 cm) away from that of 6(b). In all three of these power delay profiles, there is seen to be a weak pulse at 2 ns having a normalized amplitude of about 0.1 just before the strong pulse at about 7 ns. This weak pulse is believed to be a direct path through walls that block the LOS path. The normalized amplitude of the dominant pulses near 7 ns in Fig. 6(b) is twice as strong as that in 6(a), while in Fig. 6(c), the dominant pulse has split into two pulses having amplitudes that are much bigger than that of pulses in Figs. 6(a) and (b). This result suggests that subpaths of dominant pulses in Fig. 6(a) and (b) interfere destructively.

Fig. 7(a)–(c) shows other examples of the lightly obstructed category in the retail store. The receiver at the site "kse1" is 61.9 m (203 ft) away from the transmitter and does not have any clutter around it except for a vertical support column that is at a distance of 2.44 m from the receiver. The receiver positions are separated by one wavelength (12.3 cm) from each other along a straight line which is at an angle of about 40° to the direct path. In all of these pulse responses, two distinct pulses always exist at 5 and 43 ns. The first perceptible signal travels along a direct path from the transmitter to the receiver, so that the next strong pulse at 43 ns corresponds to a reflected ray whose path length is 12 m greater than the direct ray. From the floor plan of the retail store in Fig. 4, it is surmised that the glass wall at the entrance to the building is the source of the reflection. The responses in lightly cluttered environments, as compared to the LOS case, are characterized by a few additional strong pulses arriving tens of ns after the first observable pulses and by low amplitude echoes arriving over a longer interval out to 140 ns.

Power delay profiles of Fig. 8 are examples of the response in a heavily cluttered environment. The first two responses of Fig. 8 were obtained in the engineering building, the last two in the retail store. For responses of Fig. 8(a) and (b), the receiver was located in the center of the passage way between cubicles at the site marked "s4" in Fig. 3, which was at a distance of 40 m (121.3 ft) from the transmitter. The separation

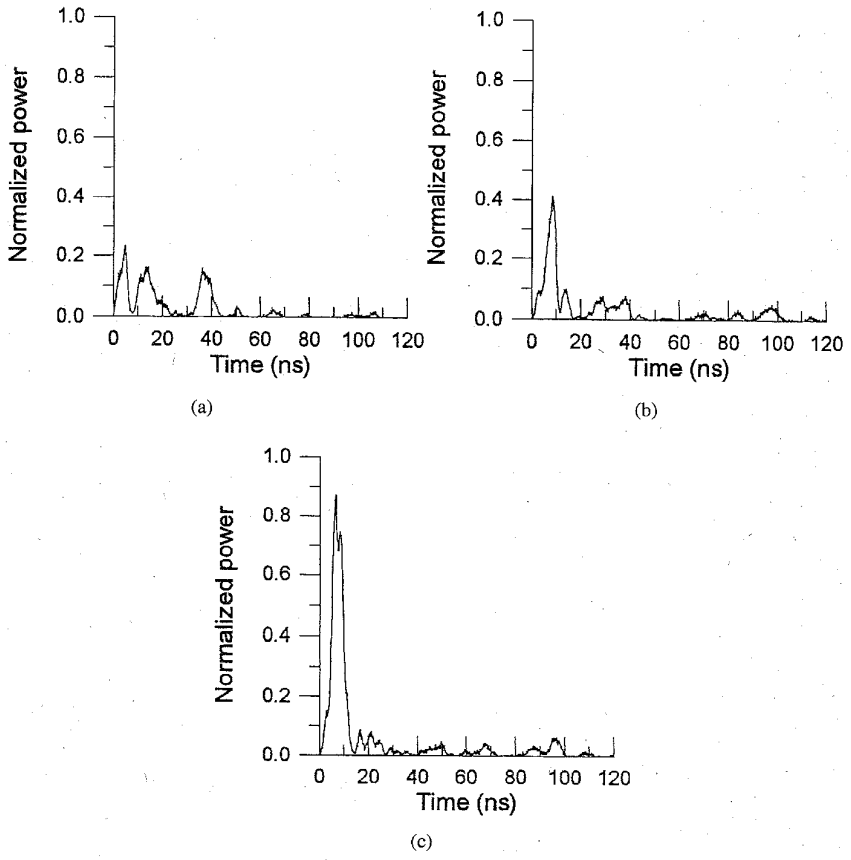

Fig. 6. Power delay profiles for a site with lightly obstructed paths to the transmitter in the engineering building.

between the receiver position corresponding to Fig. 8(a) and (b) was one wave length (12.3 cm) along a straight line parallel to the direct line between the transmitter and the receiver. In Fig. 8(a) and (b), there exist so many strong pulses that no one pulse dominates the response. The pulse near 20 ns in Fig. 8(a) seems to be the strongest and overlaps with adjacent pulses. The amplitude of this pulse drops so much in Fig. 8(b) that it is believed to be composed of many subpaths. This result can be explained by the postulate that phase differences between these subpaths change with movement of the receiver position, and as a result the amplitude of the superposition of the subpaths also changes. An examination of pulse responses at all of the 16 different receiver positions at this site reveals that none of the pulses have the same amplitude at all receiver positions. In addition to the amplitude variation of the strong pulses, the weak pulses appearing in late time of the response also vary in amplitude as the receiver is moved.

The measurements of Fig. 8(c) and (d) were made at the receiver site "kw1" in Fig. 4. There are no walls between the transmitter and the receiver, but the direct path is blocked by shelves filled with sales items. The pulse response in Fig. 8(d) was obtained at a position that was one wavelength (12.3 cm) from the position corresponding to Fig. 8(c), along the line perpendicular to the line between two antennas. Power delay profiles of Fig. 8(c) and (d) show similar behavior to those of Fig. 8(a) and (b), although the number of pulses having a significant amplitude is less. This difference may be explained by the fact that reflecting walls are much further away from the receiver and the transmitter in the retail store than in the engineering building, so that the reflected pulses are considerably weaker in the retail store.

All the responses shown in Fig. 8 consist of many pulses extending to very late times of up to 300 ns. Comparing results for three categories (LOS, light clutter, and heavy clutter) discussed above, we conclude that the characteristic of the impulse response depends primarily on the building structure and clutters between the transmitter and the receiver rather than on the distance between them.

B. Pulse Height Statistics

For a multipath channel, the pulse response can be thought of as the sum of individual pulses arriving along ray paths with ray field amplitudes α_k, delay time τ_k, and phase shift θ_k. The received signal can therefore be written as

$$x(t) = \sum_k \alpha_k e^{j(\theta_k - \omega\tau_k)} p(t - \tau_k) e^{j\omega t} \tag{1}$$

where ω is the angular carrier frequency and $p(t)$ is the amplitude variation of the individual received pulses shown

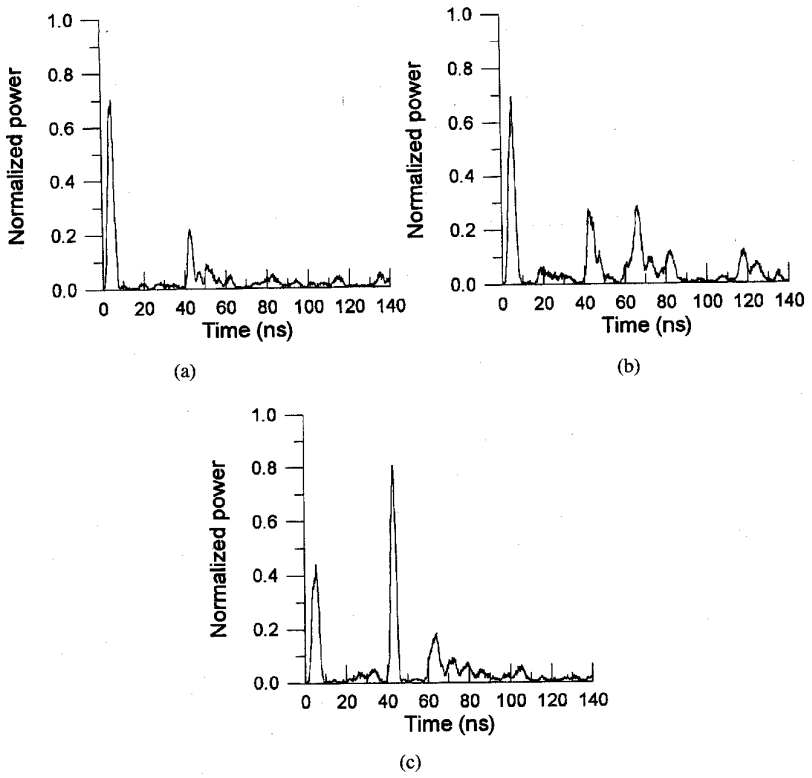

Fig. 7. Power delay profiles for a site with lightly obstructed paths to the transmitter in the retail store.

in Fig. 2(a) [13], [18]. The received signal after the envelope detector is $|x(t)|$ and can be written as

$$|x(t)| = \left\{ \sum_k \sum_l \alpha_k \alpha_l p(t-\tau_k) \times p(t-\tau_l) e^{j(\theta_k - \theta_l - \omega\tau_k + \omega\tau_l)} \right\}^{1/2}. \quad (2)$$

If no two pulses overlap in time, then the product $p(t-\tau_k)p(t-\tau_l)$ vanishes for $k \neq l$, in which case

$$|x(t)| = \sum_k \alpha_k p(t-\tau_k). \quad (3)$$

Changes in the location of the receiver that are on the order of a wavelength will cause small changes in τ_k that are on the order of the period $1/f$ of the carrier, which is less than the pulse width T. Under the assumption of nonoverlapping pulses, $|x(t)|$ in (3) will display only small time shifts as the receiver is moved. However, if the pulses overlap in time, the phase change $\exp[j\omega(\tau_l - \tau_k)]$ in (2) will cause the sum of the overlapping pulses to vary in amplitude. Because the measured pulse response $|x(t)|$ is found to exhibit large changes in the amplitude of the individual peaks as the receiver position is changed, we conclude that many individual path contributions overlap in time even for the very short 5 ns pulses used in these measurements. A statistical investigation of this variation in the amplitude of the individual peaks will therefore be helpful in simulating channel characteristics [17]–[19].

The measured pulse response contains individual peaks that can be identified throughout the 16 individual receiver positions at each site, but are often jagged. In order to avoid a subjective choice of peak amplitude and to accommodate all ray arrivals making up a peak, we averaged the amplitudes over time bins whose width is chosen as 6 ns so as to be slightly larger than the 5-ns pulse duration, centered at the delay time T_k. In this way, at each receiver position m, we obtain for the time bin centered at T_k an average pulse amplitude $A_{k,m}$ [10], [13]. The amplitude $A_{k,m}$ is then normalized to the average over the 16 receiver positions, i.e., to the value $\sum_m A_{k,m}/16$.

The normalized amplitudes of individual peaks were aggregated into separate data pools for LOS sites and cluttered sites in the two buildings. Fig. 9(a) and (b) represents the cumulative distribution functions of the data pools for LOS and cluttered environments in the engineering building and the retail store, respectively. For LOS paths in both buildings, it is seen from Fig. 9(a) and (b) that the distribution of peak amplitudes are close to the Rician distribution curve with $K = 5$, where K is the ratio of the dominant signal to the standard deviation of other weaker and randomly varying signals [20]. At the cluttered sites, the measured distribution seems to follow the Rician curve with $K = 2$, which is very close to the Rayleigh distribution [17], [20]. The differences in the

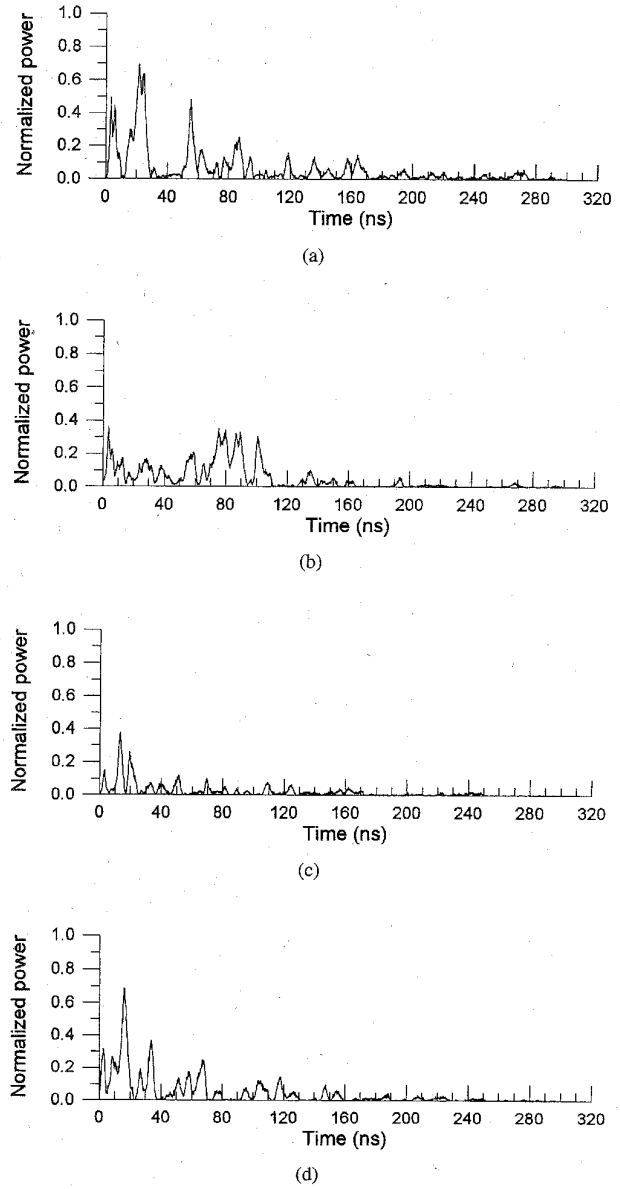

Fig. 8. Power delay profiles for sites with heavily obstructed paths to the transmitter (a) and (b) in the engineering building and (c) and (d) in the retail store.

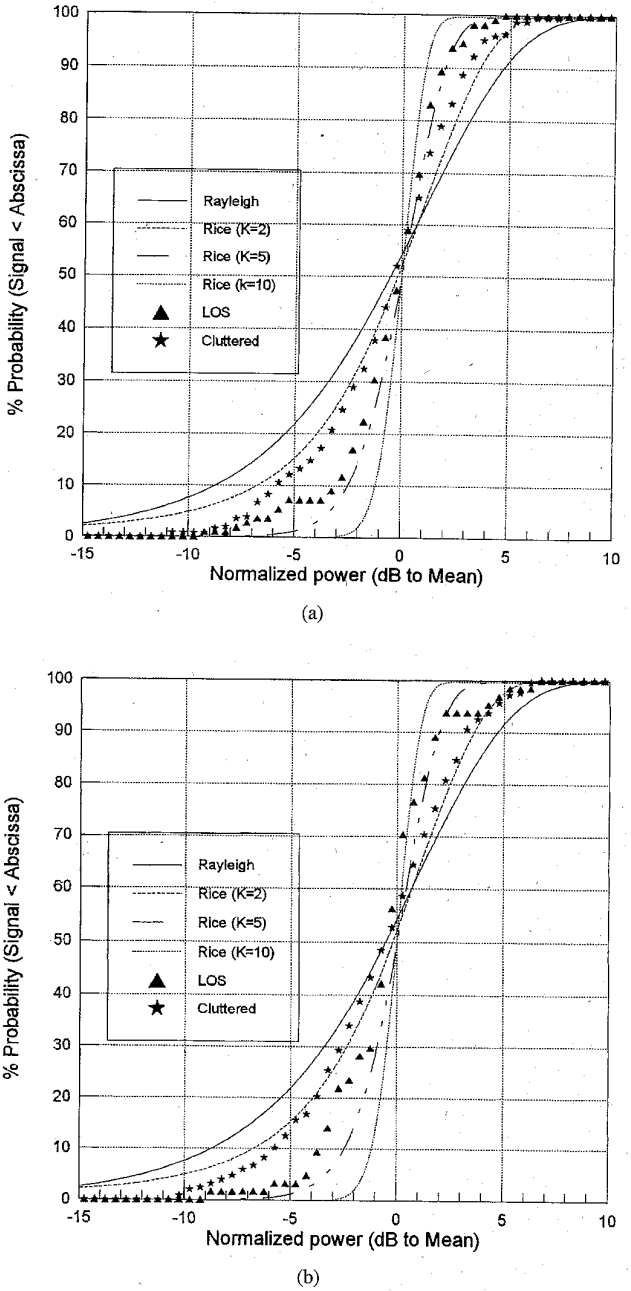

Fig. 9. Cumulative distributions of peak amplitudes. (a) Engineering building. (b) Retail store.

distributions for the LOS and for the cluttered environments is similar to that observed for CW excitation [12].

IV. Data Analysis and Discussion

A. Definitions of Channel Parameters

Multipath channels are often described by three simple parameters, which are the power gain, mean excess delay, and rms delay spread [1], [2], [5], [6], [9], [10]. In terms of the measured power delay profile $s(t) = |x(t)|^2$ the power gain is defined as

$$G = \int_{-\infty}^{\infty} s(t)\,dt. \tag{4}$$

The mean excess delay $\bar{\tau}$ is defined as

$$\bar{\tau} = \frac{\int_{-\infty}^{\infty} ts(t)\,dt}{\int_{-\infty}^{\infty} s(t)\,dt} \tag{5}$$

where $\bar{\tau}$ depends on the time origin. In this discussion we take the time origin to be at the rising edge of the first perceptible pulse. With the expression for the mean excess delay, the rms delay spread σ is found from

$$\sigma^2 = \frac{\int_{-\infty}^{\infty} (t-\bar{\tau})^2 s(t)\,dt}{\int_{-\infty}^{\infty} s(t)\,dt}. \tag{6}$$

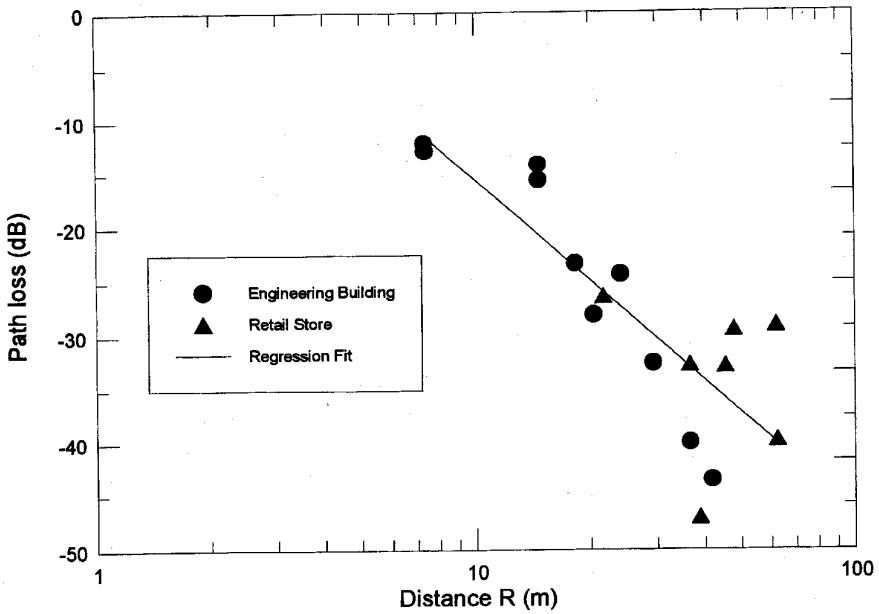

Fig. 10. Path loss relative to a 10-λ antenna separation obtained from power delay profiles.

The rms delay spread is a parameter used to determine data rates so as to avoid an intersymbol interference.

B. Path Loss

For narrow band or CW excitation, path loss is frequently discussed in terms of the sector averaged signal, which is obtained by averaging the received power as the portable is moved over a path whose length is 10λ or more. When the transmitter and the receiver are located in the clutter, the spatial average should be carried out over both the transmitter and the receiver positions [22]. However, if the transmitter is located above the clutter and away from reflecting walls, as was the case at least in the retail store, it is sufficient to average only over the receiver position.

For pulse excitation, the path loss is defined in terms of the average gain $\langle G \rangle$ at a site, which is the average of the individual gain G defined in (4) for the 16 receiver positions. To eliminate antenna gain effects, the average is normalized to the gain $G_{10\lambda}$ for an antenna separation of 10λ. In terms of $\langle G \rangle$ and $G_{10\lambda}$, the path loss for pulse excitation is

$$LP_d = A_d - A_{10\lambda} + 10 \log \frac{\langle G \rangle}{G_{10\lambda}} \tag{7}$$

where A_d is the attenuator setting used for the measurement site at a distance of d m from the transmitter and $A_{10\lambda}$ is the setting for the antenna separation of 10λ.

In processing the power delay profiles to find $\langle G \rangle$, it is important to remove contributions from noise power in the late time portion of the power profile where there are no identifiable pulse arrivals. To remove noise power, the signal level below a threshold value was set to zero. The threshold was chosen to be the greater of the following two signal levels: 1) 20 dB below the highest peak in the response and 2) the sum of the average level of the last 500 data points (corresponding to 50 ns) plus twice their standard deviation.

The path loss is plotted versus the horizontal separation R between the transmitter and the measurement site in Fig. 10. The least mean squares fit line in Fig. 10 has a slope corresponding to a path loss index $n = 3.086$ with standard deviation of 5.84 dB. This result is consistent with previous measurements reported for other buildings [5], [10], [12], [15], [21].

C. Mean Excess Delay and RMS Delay Spread

In order to calculate the mean excess delay and the rms delay spread $\bar{\tau}$ and σ, the noise power was removed from the power delay profile $s(t)$ using the thresholding technique described in the previous section. From this modified version of $s(t)$, $\bar{\tau}$ and σ are computed using (5) and (6), respectively.

Table I(a) lists the average of the mean excess delays $\bar{\tau}$ for the 16 receiver positions at each measurement site in the engineering building, as well as the standard deviation, the minimum, and the maximum of these 16 values. For comparison, the mean excess delay found from the spatial average power profile $\langle s(t) \rangle$ is also listed. Table I(b) has a similar listing for the rms delay spreads σ. Examining both mean excess delays and rms delay spreads for a site with a LOS path and a site with lightly obstructed paths to the transmitter reveals that σ is larger than $\bar{\tau}$ by about 15 ns for a LOS and about 13 ns for a lightly obstructed path to the transmitter. This results from the fact that the power delay profiles in these two environment are dominated by the first few strong pulses in the early time, which heavily influence $\bar{\tau}$, while there are many weak pulses in the late time that strongly influence σ. However, at receiver sites having heavily obstructed paths, the rms delay spread is larger than the mean excess delay by only 3 to 12 ns. For this case, the power delay

TABLE I
MEASURED PARAMETERS (ns) IN THE ENGINEERING BUILDING. (a) MEAN EXCESS DELAY. (b) rms DELAY SPREAD

	LOS path				Lightly obstructed path			Heavily obstructed path		
	east1	east2	s1	s2	east3	ne1	nw1	s3	s4	sw1
average of $\bar{\tau}$ for 16 measurement points	29.90	14.15	29.71	23.27	43.67	31.49	56.59	58.83	82.30	80.75
std. dev. of $\bar{\tau}$	8.60	5.03	8.30	8.28	14.22	7.53	15.91	10.91	11.87	15.08
max of $\bar{\tau}$	46.71	25.23	44.36	46.47	66.76	51.21	84.25	77.41	102.54	110.62
min of $\bar{\tau}$	18.62	8.40	15.03	13.40	20.31	19.99	29.96	42.19	62.20	62.02
$\bar{\tau}$ of average profile	31.66	16.03	31.29	28.20	46.39	31.34	59.39	60.76	86.39	83.48

(a)

	LOS path				Lightly obstructed path			Heavily obstructed path		
	east1	east2	s1	s2	east3	ne1	nw1	s3	s4	sw1
average of σ for 16 measurement points	44.27	23.06	44.41	39.25	55.68	46.57	59.10	55.14	69.24	67.73
std. dev. of σ	12.86	10.20	13.77	13.89	12.73	10.44	13.28	8.84	9.57	9.65
max of σ	67.85	43.00	65.11	70.52	74.88	72.10	78.86	73.59	81.64	84.60
min of σ	23.51	12.85	20.23	16.08	28.78	31.86	34.73	42.38	52.66	52.99
σ of average profile	42.00	25.21	41.62	43.35	56.25	41.04	62.96	58.12	74.51	69.79

(b)

TABLE II
MEASURED PARAMETERS (ns) IN THE RETAIL STORE. (a) MEAN EXCESS DELAY. (b) rms DELAY SPREAD

	LOS path		Lightly cluttered			Heavily cluttered	
	ke1	kn1	kse1	ksw1	kw2	kne1	kw1
average of $\bar{\tau}$ for 16 measurement points	23.21	34.29	77.15	78.82	70.55	109.70	77.22
std. dev. of $\bar{\tau}$	12.26	8.20	14.94	16.90	23.61	17.00	21.91
max of $\bar{\tau}$	49.64	44.78	98.71	113.75	117.00	142.99	124.24
min of $\bar{\tau}$	12.62	20.78	52.16	57.84	36.67	89.59	42.79
$\bar{\tau}$ of average profile	16.60	29.40	78.69	83.09	71.00	117.35	83.37

(a)

	LOS path		Lightly cluttered			Heavily cluttered	
	ke1	kn1	kse1	ksw1	kw2	kne1	kw1
average of σ for 16 measurement points	34.67	48.12	75.17	65.86	67.49	81.65	73.25
std. dev. of σ	18.14	14.86	10.41	11.61	13.74	10.33	17.02
max of σ	73.40	67.99	96.53	84.42	88.13	102.44	100.16
min of σ	20.74	25.42	53.39	47.08	40.13	57.86	42.08
σ of average profile	22.41	33.73	73.57	73.58	63.57	90.23	83.92

(b)

profiles are composed of many pulses arriving over about 200 ns, as seen in Figs. 8(a) and (b), so that pulses arriving long after the early pulses play an important role in determining both $\bar{\tau}$ and σ [2], [5], [6], [10].

It is seen from Table I(a) that measurement sites that have a LOS path to the transmitter have a somewhat smaller variation of the mean excess delays than those having an obstructed path. This observation can be explained by the fact that amplitudes of the dominant pulses in the early times of the power delay profiles show less variations at LOS sites than they do at lightly obstructed sites. Among the three lightly obstructed measurement sites in the engineering building, site "ne1" has the smallest standard deviation and is the least cluttered. The reverse situation is found for the rms delay spread. The range of variation of σ is somewhat less at heavily obstructed sites than it is at lightly obstructed and LOS sites. It is thought that the presence of many pulses makes the rms delay spread for a heavily obstructed path less sensitive to variations of the amplitude of any one pulse.

Comparing the average $\bar{\tau}$ and σ for 16 measurement points and $\bar{\tau}$ and σ of the spatial average power profile, their differences are mostly smaller than the standard deviation of $\bar{\tau}$ and σ. This indicates that $\bar{\tau}$ and σ of the spatial average power profile can be used as representative values for the measurement site.

Table II lists the mean excess delay and the rms delay spread in the retail store. Measurement site "ke1" is thought to have a LOS path to the transmitter except for the first position, which is partially blocked by merchandising shelves. For this

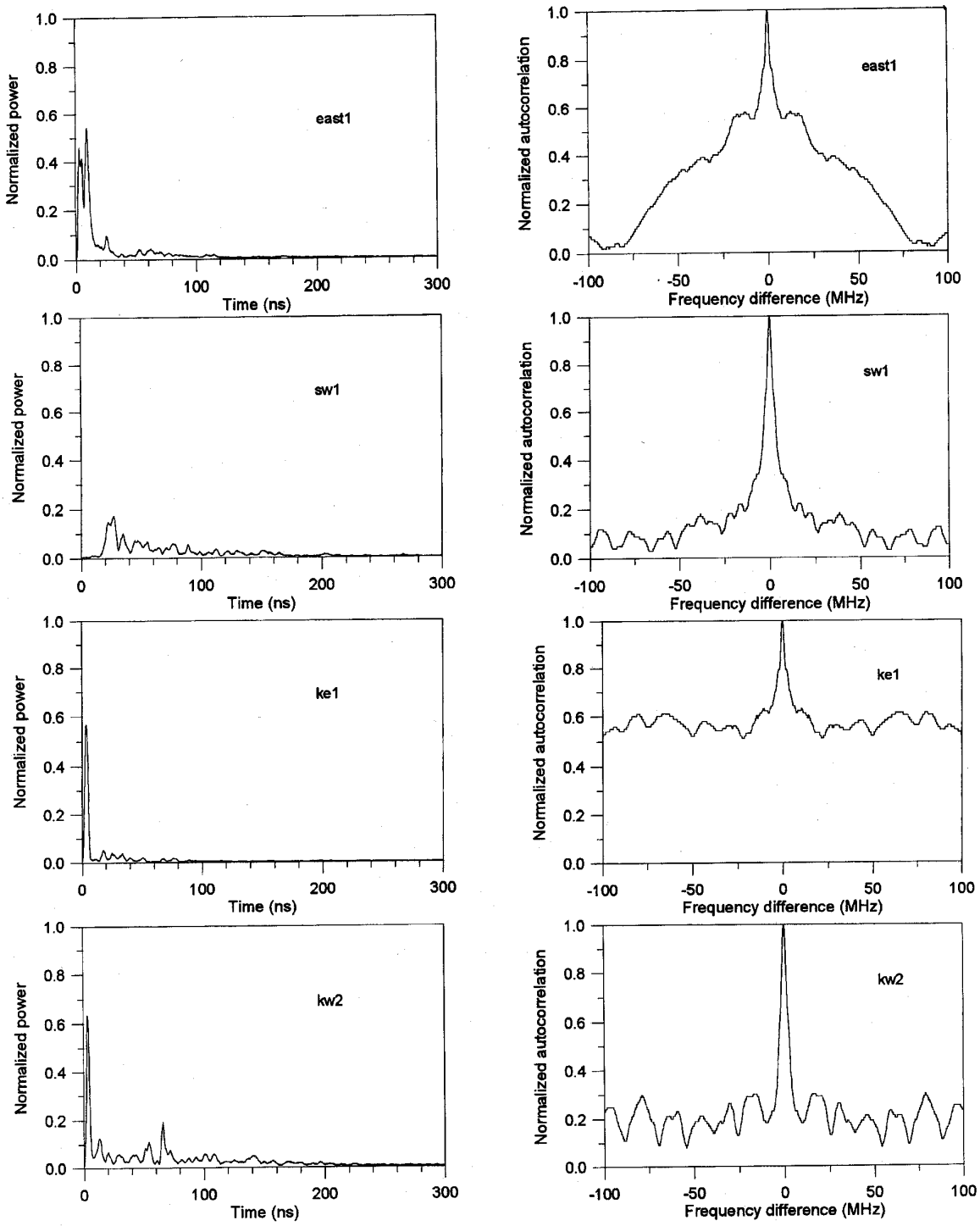

Fig. 11. Power delay profiles and their Fourier transform pairs at four measurement sites.

position the channel parameters and the power delay profile were so different from those of other positions at this site that they have been excluded in calculating the spatial average. The site "kn1" in the retail store has no obstruction except for a wooden door between the transmitter and the receiver, so that this site is assigned to the LOS path category. From Tables I and II, it is seen that the mean excess delay and the rms delay spread for LOS paths are similar for the retail store and the engineering building. The variation of σ at LOS sites in the retail store is much larger than that in the engineering building, which is due to the fact that the LOS path in the retail store suffers partial blockage of the Fresnel zone [15], so that the amplitude of the early peaks changes significantly as the receiver is moved.

TABLE III
STATISTICS OF THE rms DELAY SPREAD (ns)
FOR ALL MEASUREMENTS IN THE BUILDING

	Engineering building	Retail store
median of σ	51.5	66.5
average of σ	50.4	64.3
std. dev. of σ	17.6	20.7
maximum of σ	84.5	102.5
minimum of σ	12.5	20.5

The remaining sites in the retail store have the obstructed paths and are distinguished by the environment around the receiver. Sites "kse1," "ksw1," and "kw2" are in the lightly cluttered category because there are only a few low-height metal frame show cases around the receiver, while high merchandise shelves are far away from the receiver. Sites "kne1" and "kw1" belong to heavily cluttered category because the receiver was located between high shelves filled with various sales items. At measurement sites having obstructed paths to the transmitter, $\bar{\tau}$ is larger than σ for both lightly cluttered and heavily cluttered environments. This is similar to the result at the heavily obstructed sites in the engineering building, except that the values of the channel parameters $\bar{\tau}$ and σ in the retail store are much larger than those in the engineering building. Both $\bar{\tau}$ and σ of the spatial average power profile are not significantly different from the average $\bar{\tau}$ and σ for the 16 measurement points at each site. Thus the spatial average power profile is representative for the measurement site. However, the variation of channel parameters at a certain measurement site in the retail store is so large that the average $\bar{\tau}$ and σ are not adequate by themselves to describe the channel characteristics effectively. Comparing Tables I and II, maximum values of $\bar{\tau}$ and σ in the retail store are larger than those in the office building. This implies that the internal structure of the building is important in determining the rms delay spread.

The numerical values of the rms delay spread statistics for all measurements in each buildings are shown in Table III. In the engineering building, the median value of σ is 51.5 ns, which differs slightly from its average value, and the standard deviation is 17.6 ns. The maximum value of σ is 84.5 ns. Each numerical value of the rms delay spread statistics in the retail store is slightly higher than the corresponding value in the engineering building.

D. Coherence Bandwidth

A digital communication system operating in the ISM band can use frequency hopping as a means for mitigating against fast-fading. Packets that are not correctly received because of deep signal fading can be retransmitted at a different frequency, provided that the frequency difference is great enough so that signals are affected differently by the multipath channel. The coherence bandwidth is a measure of the minimum frequency difference such that the signals are not correlated with each other [14], [17]–[19].

To find the coherence bandwidth, let $H(f)$ be the transfer function of the channel. Since the channel varies slowly with time as people move around inside the building, or as a result of small changes in position of the mobile, $H(f)$ must be thought of a random process in the position of mobile and the observation time [18]. Then, the frequency coherence of the channel can be found from the auto correlation function defined as

$$R_H(f_1, f_2) = E[H^*(f_1)H(f_2)] \tag{8}$$

where the symbol $E[\ ]$ refers to the expected value of the random variable within the brackets. Since $H(f)$ is the Fourier transform of the impulse response $h(t)$, then

$$E[H^*(f_1)H(f_2)] = \int\int e^{j2\pi(f_1t_1 - f_2t_2)} E[h^*(t_1)h(t_2)]\, dt_1 dt_2. \tag{9}$$

If it is assumed that the impulse response $h(t)$ represents a complex-valued wide-sense stationary zero mean Gaussian random process, then the autocorrelation function $E[h(t_1)h^*(t_2)]$ vanishes for $t_1 \neq t_2$ as a result of uncorrelated scattering, so that $E[h(t_1)h^*(t_2)] = E[|h(t_1)|^2]\delta(t_1 - t_2)$ [18]. With this assumption

$$E[H^*(f_1)H(f_2)] = \int_{\infty}^{\infty} e^{-j2\pi\Delta ft} E[|h(t)|^2]\, dt \tag{10}$$

where $\Delta f = f_1 - f_2$. Defining

$$R(t) \equiv E[|h(t)|^2] \tag{11}$$

as the expectation value of the power delay profile of the channel, then

$$R_H(f_1, f_2) \equiv R_H(\Delta f) = \int_{-\infty}^{\infty} R(t) e^{-j2\pi\Delta ft}\, dt. \tag{12}$$

The coherence bandwidth is then defined as the full width of Δf at half the maximum of $R_H(\Delta f)$.

In practice, $h(t)$ in (11) can be replaced with $x(t)$ of (1) as long as a transmitting pulse duration is short compared to the delay spread. Hence, $R(t)$ in (12) can be replaced by the average power delay profile of the channel for pulse excitation $\langle s(t)\rangle$. Then, the coherence bandwidth can be determined from the measured power delay profiles using the following relationship:

$$R_H(\Delta f) = \int_{-\infty}^{\infty} \langle s(t)\rangle e^{-j2\pi\Delta ft}\, dt. \tag{13}$$

In Fig. 11, we plotted the average power delay profile and its Fourier transform defined in (13) for typical LOS sites and heavily cluttered sites both in the engineering building and in the retail store. The first two pairs in Fig. 11 reveal that the coherence bandwidth at "east1" (LOS site), at which the power delay profile has only a few additional peaks after

TABLE IV
COHERENCE BANDWIDTH OF THE CHANNELS AT THE ENGINEERING BUILDING AND THE RETAIL STORE

	Engineering building		Retail store	
	site	$\Delta f = f_1 - f_2$ (MHz)	site	$\Delta f = f_1 - f_2$ (MHz)
LOS path	east1	42.62	ke1	> 100
	east2	45.82	kn1	36
	s1	18.5		
	s2	44		
Lightly obstructed path	ne1	30.3	kse1	5.94
	east3	10.75	ksw1	7.45
	nw1	8.46	kw2	5.53
Heavily obstructed path	s3	8.85	kne1	5.03
	s4	6.5	kw1	6.71
	sw1	7.11		

the first detectable peak, is much larger than that at "sw1" (heavily cluttered site), where many pulses in late time have substantial amplitudes relative to the strongest pulse. The last two pairs in Fig. 11 represent the power delay profiles and their Fourier transforms at sites "ke1" and "kw2" in the retail store. At "ke1," power delay profile has only one large peak in early time so that the coherence bandwidth is greater than 100 MHz, which is true for most of locations at this site except for a couple of locations whose LOS path is partially blocked by obstacles, while the coherence bandwidth at the cluttered site "kw2" is comparable to that at "sw1" in the engineering building.

Table IV lists the coherence bandwidths calculated from the average power delay profile at each measurement site in the engineering building and in the retail store. In both buildings, the coherence bandwidth of most LOS sites is larger than 30 MHz, except at site "s1." The nonLOS sites in both buildings have Δf between 5 and 11 MHz, except for site "ne1" where Δf is similar to that at LOS sites.

V. CONCLUSION

In this paper we investigated indoor channel characteristics such as impulsive channel parameters, path loss, individual peak amplitude statistics, and coherence bandwidth in the 2.4-GHz ISM bands by carrying out impulse response measurements in two different buildings. For LOS paths, the first arriving pulses are direct and floor reflected rays, which interfere with each other as the receiver is moved. For sites where the direct path to the transmitter is blocked by walls, or tall obstacles such as merchandise shelves, the amplitudes of the distinguishable peaks result from the summation of many subpaths whose relative phase changes rapidly as the receiver is moved. As a result, the peak amplitudes appear to change randomly with position. For these obstructed sites, the statistical distribution of the peak amplitude is close to the Rician distribution with $K = 2$, which is only slightly different from the Rayleigh distribution.

The mean excess delay and rms delay spread were obtained from the power delay profile. Mean excess delay values were typically less than 85 ns in the engineering building and 115 ns in the retail store. On the other hand, rms delay spread values were typically less than 75 ns in the engineering building and 90 ns in the retail store. It was observed that rms delay spread depends on the extent of clutter around the receiver, as well as the nature of the propagation path between the transmitter and the receiver. Regression analysis of path loss in the two buildings gives a path loss index $n = 3.086$, which is consistent with previous measurements [5], [10], [12], [15]. The coherence bandwidth due to multipath propagation was also determined and found to range between 5 and 10 MHz for obstructed sites.

ACKNOWLEDGMENT

The authors would like to thank J. Swartz and J. Katz of Symbol Technologies, Inc. for their encouragement an support and R. Martino, Jr., also of Symbol Technologies, Inc. for his technical advice.

REFERENCES

[1] D. C. Cox, "Delay doppler characteristics of multipath propagation at 910 MHz in a suburban mobile radio environment," *IEEE Trans. Antennas Propagat.*, vol. AP-20, no. 5, pp. 625–635, Sept. 1972.
[2] D. M. J. Devasirvatham, "Time delay spread and signal level measurements of 850 MHz radio waves in building environments," *IEEE Trans. Antennas Propagat.*, vol. AP-34, no. 11, pp. 1300–1305, Nov. 1986.
[3] S. J. Patsiokas, B. K. Johnson, and J. L. Dailing, "Propagation of radio signals inside buildings at 150, 450 and 850 MHz," in *Proc. 36th IEEE Vehicular Technology Conf.*, Dallas, TX, 1986, pp. 66–72.
[4] J. Horikosh, K. Tanaka, and T. Morinaga, "1.2 GHz band wave propagation measurements in concrete building for indoor radio communications," *IEEE Trans. Veh. Technol.*, vol. VT-35, no. 4, pp. 146–152, Nov. 1986.
[5] A. A. M. Saleh and R. A. Valenzuela, "A statistical model for indoor multipath propagation," *IEEE J. Select. Areas Commun.*, vol. SAC-5, no. 2, pp. 138–146, Feb. 1987.
[6] D. M. J. Devasirvatham, "Multipath time delay spread in the digital portable radio environment," *IEEE Commun. Mag.*, vol. 25, no. 6, pp. 13–21, June 1987.
[7] Y. Yamaguchi, T. Abe, and T. Sekiguchi, "Radio propagation characteristics in underground streets crowded with pedestrians," *IEEE Trans. Electromag. Compat.*, vol. 30, no. 2, pp. 130–136, May 1988.
[8] H. W. Arnold, R. Murray, and D. C. Cox, "815 MHz radio attenuation measured within two commercial buildings," *IEEE Trans. Antennas Propagat.*, vol. 37, no. 10, pp. 1335–1339, Oct. 1989.
[9] R. Bultitude, S. Mahmoud, and W. Sullivan, "A comparison of indoor radio propagation characteristics at 910 MHz and 1.75 GHz," *IEEE J. Select. Areas Commun.*, vol. 7, no. 1, pp. 20–30, Jan. 1989.
[10] T. S. Rappaport, "Characterization of UHF multipath radio channel in factory buildings," *IEEE Trans. Antennas Propagat.*, vol. 37, no. 8, pp. 1058–1069, Aug. 1989.
[11] T. S. Rappaport, "Indoor radio communications for factories of the future," *IEEE Commun. Mag.*, pp. 15–24, May 1989.
[12] J. F. Lafortune and M. Lecours, "Measurement and modeling of propagation losses in a building at 900 MHz," *IEEE Trans. Veh. Technol.*, vol. 39, no. 2, pp. 101–108, May 1990.
[13] G. L. Turin, F. D. Clapp, T. L. Johnston, S. B. Fine, and D. Lavry, "A statistical model of urban multipath propagation," *IEEE Trans. Veh. Technol.*, vol. VT-21, no. 1, pp. 1–9, Feb. 1972.

[14] A. P. Bello and B. D. Nelin, "The effect of frequency selective fading on the binary error probability of incoherent and differently coherent matched filter receivers," *IEEE Trans. Commun. Syst.*, vol. CS-11, pp. 170–186, June 1963.
[15] W. Honcharenko, H. L. Bertoni, J. L. Dailing, J. Qian, and H. D. Yee, "Mechanism governing UHF propagation on single floors in modern office buildings," *IEEE Trans. Veh. Technol.*, vol. 41, no. 4, pp. 496–504, Nov. 1992.
[16] P. Karlsson and L. Olsson, "Time dispersion measurement system for radio propagation at 1800 MHz and results from typical environments," in *Proc. 44th IEEE Veh. Technol. Conf.*, Stockholm, Sweden, 1994, pp. 1793–1797.
[17] S. Haykin, *Communication Systems*. New York: Wiley, 1983, ch. 5.
[18] J. G. Proakis, *Digital Communications*. New York: McGraw-Hill, 1989, pp. 702–719.
[19] W. C. Y. Lee, *Mobile Communications Engineering*. New York: McGraw-Hill, 1982, chs. 1–3, 6.
[20] B. P. Lathi, *Modern Digital and Analog Communication Systems*. Philadelphia, PA: Holt, Rinehart and Winston, 1989, pp. 435–450.
[21] T. S. Rappaport and C. D. Mcgillen, "UHF fading in factories," *IEEE J. Select. Areas Commun.*, vol. 7, no. 1, pp. 40–48, Jan. 1989.
[22] W. Honcharenko, H. L. Bertoni, and J. L. Dailing, "Bilateral averaging over receiving and transmitting areas for accurate measurements of sector average signal strength inside buildings," *IEEE Trans. Antennas Propagat.*, vol. 43, no. 5, pp. 508–512, May 1995.

Henry L. Bertoni (M'67–SM'79–F'87) was born in Chicago, IL, on November 15, 1938. He received the B.S. degree in electrical engineering from Northwestern University, Evanston, IL, in 1960. He was awarded the M.S. degree in electrical engineering in 1962 and the Ph.D. degree in electrophysics in 1967, both from the Polytechnic Institute of Brooklyn (now Polytechnic University).

After graduation he joined the faculty of the Polytechnic, becoming Head of the Electrical Engineering Department. He is now the Vice Provost of Research and Graduate Studies. His research has dealt with theoretical aspects of wave phenomena in electromagnetics, ultrasonics, acoustics, and optics. He has authored or co-authored over 100 journal and proceedings papers on these topics. During 1982–1983 he spent sabbatical leave at University College London as a Guest Research Fellow of the Royal Society. The research he carried out at University College was the subject of a paper that was awarded the 1984 Best Paper Award of the IEEE Sonics and Ultrasonics Group. During the summer of 1983 held a Faculty Research Fellowship at USAF Rome Air Development Center, Hanscom AFB, MA. His current research in electromagnetics deals with the theoretical prediction of UHF propagation characteristics in urban environments, and he and his students were the first to explain the mechanisms underlying characteristics observed for propagation of the cellular mobile radio signals. One of his papers on this topic received the 1993 Neal Shepherd Best Propagation Paper Award of the IEEE Vehicular Technology Society.

Dr. Bertoni was the first Chairman of the Theoretical Committee on Personal Communications of the IEEE Communications Society and IEEE representative to and Chairman of the Hoover Medal Board of Award. He has served on the ADCOM of the IEEE Ultrasonics, Ferroelectric and Frequency Control Society, and is also a member of the International Scientific Radio Union and the New York Academy of Science.

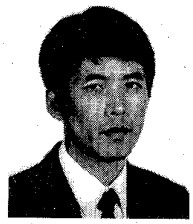

Seong-Cheol Kim was born in Taegu, Korea, on May 16, 1961. He received the B.S. and M.S. degrees in electrical engineering from Seoul National University, Seoul, Korea, in 1984 and 1987, respectively. He received the Ph.D. degree in electrical engineering from the Polytechnic University, Brooklyn, NY, in 1995.

From 1985 to 1987 he was a Research Assistant in the Plasma Engineering Laboratories in the Electrical Engineering Department at Seoul National University. Since 1991 he has worked for Center for Advanced Technology in Telecommunications at Polytechnic University with a grant from Symbol Technologies, Inc. During the summers of 1992–1994, he carried out experiments on the characterization of the indoor CW and pulsed radio propagation at Symbol Technologies, Inc., Bohemia, NY. He is now in the Wireless Communications Systems Engineering Group at AT&T Bell Laboratories, Holmdel, NJ. His research interests cover the characterization and modeling of radio wave propagation in buildings and urban environments for PCS and wireless Data Communication and the deployment of wireless communication systems.

Dr. Kim is a member of Eta Kappa Nu.

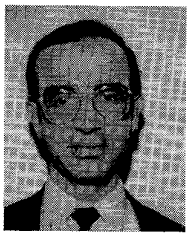

Miklos Stern (S'80–M'80) was born in Budapest, Hungary, in 1957. He received the B.S. degree from Polytechnic Institute of New York in 1981 and M.S. and Ph.D. degrees from Columbia University, New York, in 1982 and 1990, respectively, all in electrical engineering.

In 1982 he joined Bell Laboratories, where he worked on digital communication systems. From 1984 until 1992 he was with Bellcore, where he was engaged in lightwave communication system research. He studied subpicosecond pulse transmission in optical fibers for ultra-high-speed data transmission applications. He was also responsible for implementing an experimental multi-Gbit/s fiber-optic transmission system based on the SONET/ATM communication protocols. He is currently a Member of Technical Staff of the Research Department at Symbol Technologies in Long Island, New York. His current interests are laser scanning and wireless communications. He authored of co-authored more than 30 technical publications and conference papers and has several patents issued or pending.

Dr. Stern is a member of the Optical Society of America.